

Effects of temperature distribution on plasticity in laser dieless drawing

YONGGANG LI

School of Optic/CREOL (Center for Research and Education of Optics and Lasers), Mechanical, Materials and Aerospace Engineering Department, University of Central Florida, Orlando, FL 32816-2700, USA

N. R. QUICK

PALL Corporation, Fluid Dynamics Division, Inc., 1750 Filter Drive, DeLand, FL 32724-2045, USA

A. KAR

School of Optic/CREOL (Center for Research and Education of Optics and Lasers), Mechanical, Materials and Aerospace Engineering Department, University of Central Florida, Orlando, FL 32816-2700, USA
E-mail: Aravinda@creol.ucf.edu

Temperature measurement based on grey body radiation spectrum is used to determine the temperature profile of hot wires in the deformation region in laser dieless wire drawing, with spatial resolution down to a few micrometers. The Voce parameters characterizing the high temperature plastic flow behavior of the wires are calculated using the temperature and diameter profiles of the wires in the deformation region. These parameters are determined for as-drawn and annealed pure nickel wires of 500 μm diameter.

Recrystallization and grain growth during the drawing process are studied. The effects of temperature, grain size and precursor wire diameter on wire drawability and strain rate are analyzed. The measured temperature and diameter profiles agree well with theoretical results. Grain growth increases rapidly with increasing temperature after recrystallization, and the grain size follows the thermal activation law. The effective activation energy increases for larger wire diameter. Surface morphology of the drawn wires and strain rate calculation show that dislocation motion is the dominant deformation mechanism.

© 2003 Kluwer Academic Publishers

1. Introduction

Laser-assisted forming takes advantages of reduced material strength, increased formability and/or laser-induced thermal deformation. Laser bending has been extensively investigated and implemented for industrial applications since the initial work by Namba [1]. In recent years, laser-assisted deep drawing of metal sheets has been analyzed by Schuöcker *et al.* [2, 3]. More recently, a flexible dieless wire drawing technique using laser beam heating was developed by Li *et al.* [4]. Laser dieless wire drawing utilizes the enhanced plasticity at elevated temperatures. The material undergoes a transition region in which the wire temperature changes significantly to allow plastic flow. Process optimization and control require the understanding of the temperature distribution at the transition region and the high temperature plasticity of the material. Li *et al.* [5] presented a one-dimensional thermomechanical model to predict the temperature and deformation profiles for laser dieless drawing and compared the radius profile and drawing force with experimental data. No experimental temperature data were available at that time to

verify the thermal model, and also the mechanical parameters in Voce's plastic flow equation were chosen arbitrarily in the thermomechanical model. An accurate constitutive law for the mechanical behavior of a material is rarely available over a wide range of temperature due to numerous variables, such as grain size, recrystallization, grain growth, and strain hardening, affecting such behavior. Generally, an empirical relation, e.g., Voce's equation, is developed containing several unknown parameters. Determination of these parameters through routine mechanical test is costly and time-consuming. Temperature measurement and mechanical parameter determination are thus necessary to understand the properties of materials at high temperatures. Since the wire sample in the present case is small, encased in a protection environment, and in motion, a non-contact method based on thermal emission is used for temperature measurement in this study enabling point-to-point temperature testing along the wire. A method is presented to calculate the Voce parameters of the wire sample based on the radius profile in the deformation region during laser dieless drawing.

The drawability of nickel 200 wires of different diameters and heat-treatment conditions was investigated by the authors in [6] leading to the following observations: (1) For the same precursor wire, the drawability increases with the maximum temperature T_{\max} (which is proportional to the incident laser power) to a maximum and then decreases as T_{\max} continues to increase; (2) The drawability is better for as-drawn precursor wire than for the annealed one of the same diameter at the same drawing conditions; and (3) The drawability degrades as the precursor wire diameter decreases. In this paper, the relationship between temperature, grain growth, deformation mechanism and plasticity is analyzed to understand the above observations.

2. Experiments

2.1. Wire drawing experiments

The laser wire drawing experimental setup is shown in Fig. 1. Two translation stages are used for wire feeding and pulling separately to draw a finite segment of a precursor wire into a smaller diameter wire. A load cell is used to measure the drawing force. Precursor nickel 200 wires of 500 μm nominal diameter, as-received in both as-drawn and annealed conditions, were laser-drawn for different laser powers and different drawing ratios to study their effects on drawability, drawing force and microstructures. Three as-drawn precursor wires of nominal diameters 500, 125 and 50 μm were also tested for microstructure and drawability to study the effect of initial diameter. The wire feeding rate was $v_i = 300$ mm/min and the length of the precursor wire was 600 mm in all cases. A continuous wave, Gaussian Nd:YAG laser beam was used to heat the wire. It is necessary to ensure the quality of the laser beam in order to compare the experimental data with theoretical results obtained by using the thermomechanical model developed in [5] based on a Gaussian laser beam. The laser beam profile before the focusing lens was measured using a profilometer and is shown in Fig. 2. This laser beam was then focused to an elliptical spot of major axis $2a$ and minor axis $2b$ on a horizontal plane

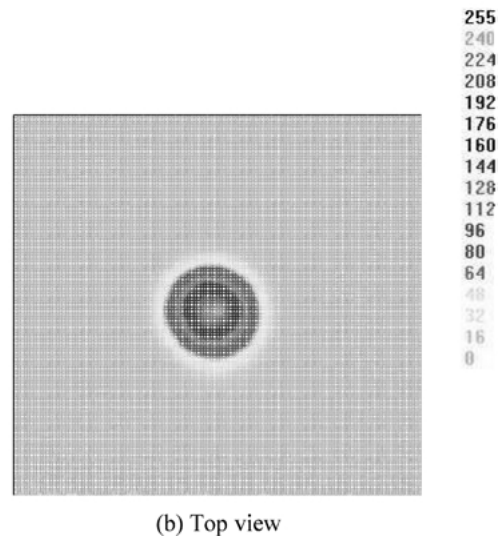
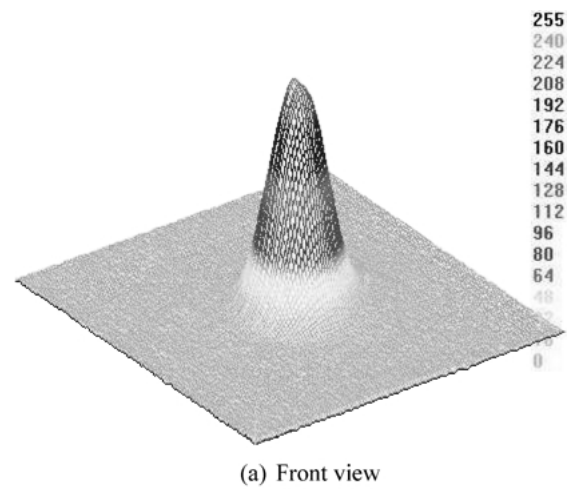


Figure 2 Intensity profile of the incident laser beam showing good Gaussian quality.

tangential to the top of the wire. The spot size is $2a = 5$ mm and $2b = 0.014$ mm produced by a cylindrical lens for nickel wires of 500 μm nominal diameter, and $2a = 2b = 1.0$ mm produced by a spherical lens for the other two precursor wires. A drawing cell (Fig. 1)

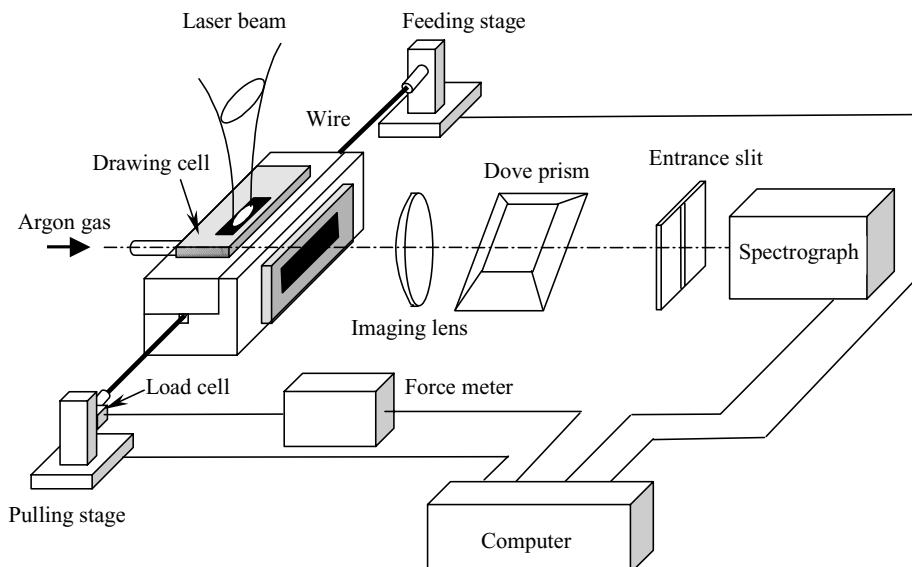


Figure 1 Wire drawing experimental setup incorporating instruments for drawing force and wire temperature measurements.

was used to align the wire with the incident laser beam and prevent the wire from oxidation by continuously flowing argon through the cell at a constant flow rate of 50 liter/min.

2.2. Temperature measurement

Wire temperature measurement is carried out by recording the radiation spectrum of the wire and calculating the temperature based on Planck's equation for blackbody radiation. Since the wire temperature is below its melting point, the radiation spectrum follows a continuum. For a real body, the ratio of spectral radiation powers $I_1(\lambda_1, T)$ and $I_2(\lambda_2, T)$ can be written as

$$\frac{I_1(\lambda_1, T)}{I_2(\lambda_2, T)} = \frac{\varepsilon_1(\lambda_1, T)}{\varepsilon_2(\lambda_2, T)} \frac{\lambda_2^5 (e^{\frac{hc}{\lambda_2 k_B T}} - 1)}{\lambda_1^5 (e^{\frac{hc}{\lambda_1 k_B T}} - 1)} \quad (1)$$

from which T can be written explicitly as

$$T = \frac{hc}{k_B} \frac{\frac{1}{\lambda_2} - \frac{1}{\lambda_1}}{\ln\left(\frac{I_2}{I_1}\right) + 5 \ln\left(\frac{\lambda_2}{\lambda_1}\right)} \quad \text{for } \frac{hc}{\lambda_i k_B T} \gg 1, i = 1, 2 \quad (2)$$

and $\varepsilon_1(\lambda_1, T) = \varepsilon_2(\lambda_2, T)$ for $\lambda_1 \approx \lambda_2$.

$\varepsilon_1(\lambda_1, T)$ and $\varepsilon_2(\lambda_2, T)$ are emissivities of the object at wavelengths λ_1 and λ_2 , respectively, and temperature

T . Assuming that the emissivity does not change with the wavelength (blackbody and greybody), the temperature of the object can be calculated from Equation 1, which is referred to as two-color temperature [7, 8].

Emission spectroscopy is used to measure the wire temperature. The radiation emitted by the laser-heated segment of the wire is recorded using an optical system that includes an imaging optics and a multichannel spectrograph (optical multichannel analyzer (OMA)). The spectrograph has a vertical entrance slit whose width can be adjusted down to 10 μm . The imaging lens serves to image and magnify the wire at the entrance slit of the spectrograph through a dove prism. The dove prism rotates the horizontal wire into vertical position to line-up with the vertical entrance slit. Depending on the magnification of the imaging optics, the height of the wire image on the CCD camera of the spectrograph varies from a few to about 20 mm. OMA can be operated in either image or spectrograph mode. The image of a segment of the wire is captured in the image mode as shown in Fig. 3a. The spectrum of the radiation emitted by the laser-heated wire can be recorded for any sub-region within the image area. Larger area is preferred for higher signal-to-noise ratio. The heated region is divided into several smaller

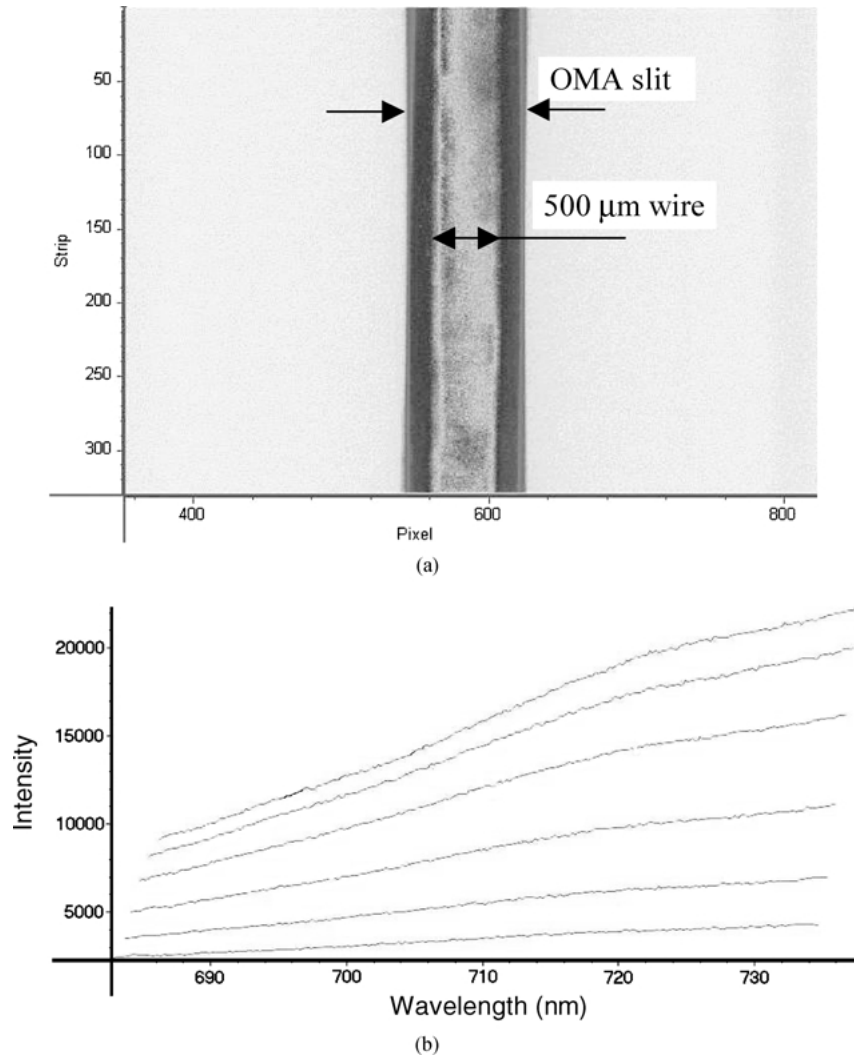


Figure 3 (a) Wire image and (b) emission spectra from six sub-regions in the deformation region of the wire in laser dieless drawing. Nickel 200 wire of 500 μm diameter, spectrograph entrance slit width: 1.2 mm.

regions, each having an area of $0.2 \text{ mm} \times 0.26 \text{ mm}$. The spacing of these regions is 1 mm , and spectra are captured for six consecutive regions with the same exposure as shown in Fig. 3b. The spectra are stored in a computer connected to the spectrograph, and the optics-spectrograph assembly translates 6 mm along the wire to capture the spectra for the neighboring six regions. Eighteen regions were investigated in the deformation region for each wire covering 17 mm long segment of the wire. The temperature in each region is calculated using the spectrum by the two-color temperature method.

2.3. Mechanical parameter determination

The Voce empirical relation [9], which accounts for the variation of the stress with the strain, strain rate and temperature, is often used to present the plastic deformation of the wire being drawn, i.e.,

$$\sigma(\varepsilon, \dot{\varepsilon}, T) = [\sigma_1 - (\sigma_1 - \sigma_0) \exp(-n\varepsilon)] \times \exp\left(-\kappa \frac{T}{T_M}\right) \left(\frac{\dot{\varepsilon}}{\dot{\varepsilon}_0}\right)^m \quad (3)$$

where n is the strain-hardening factor whose value represents the strain-hardening of the material. m is the strain rate sensitivity which indicates the sensitivity of the flow stress to the strain rate, κ the temperature coefficient of the stress, T_M is the melting temperature of the wire, and $\dot{\varepsilon}_0$ is a scaling factor which is generally taken as 1 s^{-1} . σ_0 , σ_1 , m , n , and κ are material constants which are generally assumed to be temperature independent for simplicity. The Voce equation was used in the thermomechanical model developed in [5] for laser dieless wire drawing. All thermomechanical parameters, such as the temperature, stress, strain and strain rate, vary widely in the deformation region during the drawing process. The stress σ , strain ε , and strain rate $\dot{\varepsilon}$ can be expressed in terms of the wire radius as [5]:

$$\sigma = \frac{F}{\pi r^2} \quad (4)$$

$$\varepsilon = \ln \frac{r_i^2}{r^2} = 2 \ln \frac{r_i}{r} \quad (5)$$

$$\dot{\varepsilon} = -\frac{2v_i r_i^2}{r^3} \frac{dr}{dx} \quad (6)$$

where r is the radius at location x , r_i is the initial radius of the wire, v_i is the wire feeding velocity, and F is the wire drawing force.

The five Voce parameters in Equation 3 can be estimated using the measured drawing force, temperature distribution, and the radius profile in the deformation region. This can be done by choosing a set of points in the deformation region at which the temperature and radius are measured and the stress, strain, and strain rate are calculated using Equations 4–6. The Voce parameters are then obtained through a least square fit of these data using Equation 3.

TABLE I Voce parameters for nickel 200 wires of $500 \mu\text{m}$ nominal diameter

Wire	σ_0 (GPa)	σ_1 (GPa)	n	m	κ
Annealed	8.42	13.4	8.60	0.297	6.87
As-drawn	22.5	38.1	6.56	0.375	8.96

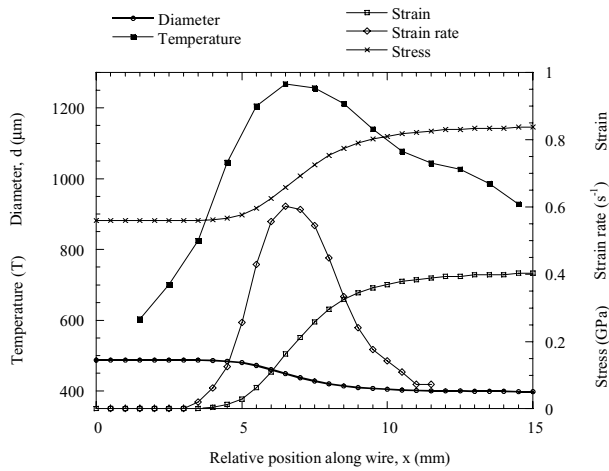
The temperature distribution was obtained from the measured spectra for both the as-drawn and annealed precursor nickel wires at laser power 24.1 W and a drawing ratio of 1.5 . The corresponding radius profiles were frozen to room temperature and measured using a micrometer with a resolution of $1 \mu\text{m}$. Fifteen points were selected in the deformation region to determine the Voce parameters by using the least square method. These parameters are listed in Table I and used in the model presented in [5] to calculate the temperature and radius profiles for other laser dieless drawing conditions. The calculated values are compared with experimental data to verify the model predictions.

3. Results and discussion

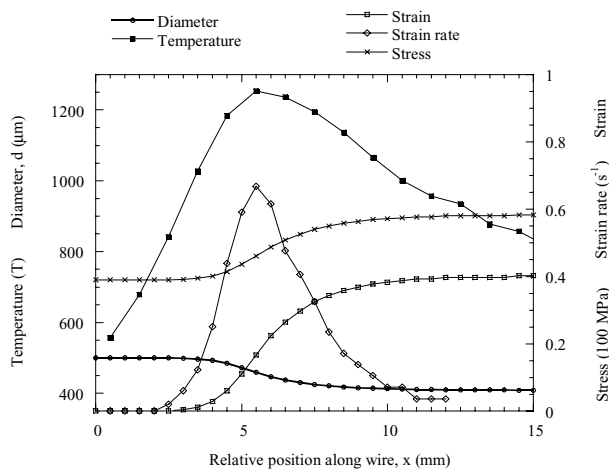
3.1. Temperature profile

Experimental temperature and radius profiles of the wire, and high temperature stress, strain and strain rate experienced by the wire during laser drawing are presented in Fig. 4 for both as-drawn and annealed precursor nickel 200 wires. The wire feeding speed was 300 mm/min and the pulling speed was 450 mm/min . Heated by a laser beam of power 24.1 W , both the annealed and as-drawn precursor wires exhibit optimal drawability. The diameter profiles in Fig. 4 correspond to these drawing conditions, and the deformation properties are obtained from the diameter profiles using Equations 4–6. The drawing force was measured by a load cell connected to the wire (Fig. 1). Since the temperature and diameter profiles were measured separately, they may not represent data at the same location of the wire. To project the data to the same location of the wire, they are plotted in Fig. 4 such that the point of maximum temperature coincides with the point of maximum strain rate, since the maximum temperature corresponds to the lowest flow stress and highest strain rate.

Fig. 4 provides all the thermomechanical variables, i.e., the temperature, stress, strain, and strain rate, appearing in the Voce Equation 3. Fifteen points were selected to determine the Voce parameters for each wire by using the least square method and the results are listed in Table I. It should be noted that these Voce parameters generally vary with temperature and deformation mechanism. The values listed in Table I can be interpreted as average values in the range of temperature, strain and strain rate experienced by the wires, and they can be used in a thermomechanical model to predict the wire temperature and deformation during laser wire drawing process. The Voce parameters obtained for as-drawn wire of $500 \mu\text{m}$ diameter are used for as-drawn wires of other diameters in this study. The Voce parameter σ_0 can be considered as the linear



(a)

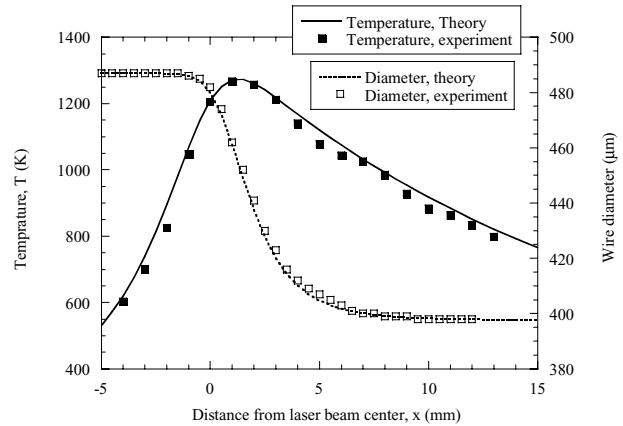


(b)

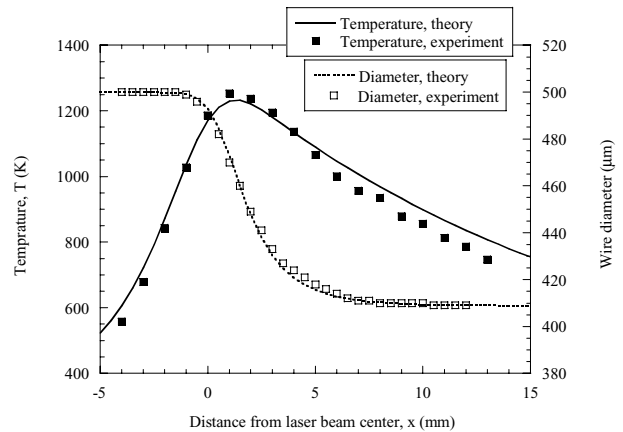
Figure 4 Experimental temperature and deformation data plotted for (a) 487 μm diameter annealed nickel and (b) 500 μm as-drawn nickel wire. $v_i = 300$ mm/min, $v_o = 450$ mm/min; laser spot size $2a = 5.0$ mm, $2b = 0.014$ mm; protection gas: argon.

limit of tensile stress at strain rate $\dot{\epsilon}_0$ and temperature 0 K. The as-drawn nickel 200 wire has a value of σ_0 much higher than the annealed wire, which is reasonable since the former is significantly strain-hardened. In fact, the room temperature tensile strength of the as-drawn wire is 986 MPa at a strain rate of 10^{-3} s $^{-1}$, while it is 488 MPa for the annealed wire. σ_1 also represents flow stress and is reasonably higher for the as-drawn wire. The strain-hardening factor (n) is larger for the annealed wire than for the as-drawn wire when subjected to plastic deformation, while the opposite is true for the temperature coefficient κ . The strain rate sensitivity m indicates the deformation mechanism and qualitatively represents the ductility of the material. A higher value of m implies more ductility. The value of m is generally in the range of 0.4–0.6 for superplastic metals, whereas other materials have much lower value of m . In this study, the as-drawn precursor wire exhibits a higher value of m than the annealed wire, which correlates with the observation that the drawability of the former is better than the latter [4, 6].

Using the thermomechanical model developed in [5] and the Voce parameters obtained in this study, the temperature and diameter profiles are calculated. The



(a)



(b)

Figure 5 Comparison of theoretical and experimental results for temperature and diameter profiles for (a) 487 μm diameter annealed and (b) 500 μm diameter as-drawn precursor nickel 200 wires. Lines show calculation results and points show experimental results. $v_i = 300$ mm/min, $v_o = 450$ mm/min laser spot size $2a = 5.0$ mm, $2b = 0.014$ mm; protection gas: argon.

results for both the as-drawn and annealed precursor wires are compared with experimental data in Fig. 5. The measured temperature distributions are slightly narrower than the model predictions. This may be partly due to the use of temperature-independent absorptivity in the theoretical calculation. The absorptivity increases with temperature, resulting in higher temperature rise in hot regions, compared to the case when the absorptivity remains unchanged with temperature.

3.2. Effect of temperature on grain size

The dependence of wire drawability on the maximum temperature generated by laser heating was studied in [6]. The drawability is very low at low temperatures for the as-drawn precursor wires of all three diameters for T_{max} below 800 K, but increases gradually with incident laser power as T_{max} reaches 800 K. The drawability reaches maximum for T_{max} in the range of 1050–1250 K and then decreases rapidly with increasing T_{max} [6]. Microstructural analysis revealed that the original unidirectionally elongated grain structure was transformed to recrystallized equiaxed microcrystalline structure at laser powers corresponding to $T_{\text{max}} \approx 800$ K, and grain growth occurred rapidly with increasing T_{max} [6]. Fig. 6 shows the variation of the grain size d_g in the wires

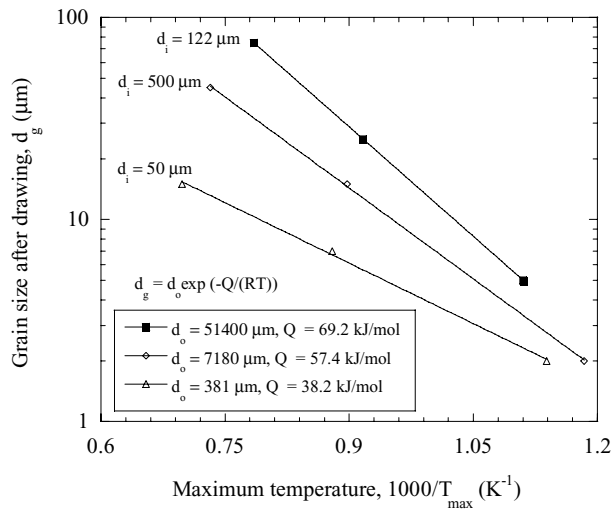


Figure 6 Grain size of the wires after being laser drawn as a function of the maximum temperature. Laser spot size: $2a = 5$ mm, $2b = 0.014$ mm for precursor wire diameter $d_i = 500$ mm, and $2a = 2b = 1.0$ mm for other diameters, $v_i = 300$ mm/min, argon protection.

after being laser-drawn for different values of maximum temperature. For the as-drawn precursor wires of three different diameters, d_g follows the typical thermal activation relation $d_g = d_o \exp(-Q/(RT))$, where Q is the effective activation energy (the term “effective” is used since the activation energy for grain growth is normally defined for an isothermal condition, whereas the temperature changes along the length of the wire in the present case), R is the universal gas constant and d_o is a pre-exponential term. Q is equal to the slope of the curves in Fig. 6 and is determined to be 69.2, 57.4 and 38.2 kJ/mol for precursor wires of diameter 500, 122 and 50 μm , respectively.

The differences in the values of Q may be due to the differences in the length of time the wires remain in the high temperature deformation region. Since grain growth starts at about 800 K, the time in which the wire remains above 800 K is taken as the time of grain growth. The grain growth time is calculated using the model of [5] and presented in Fig. 7 as a function of

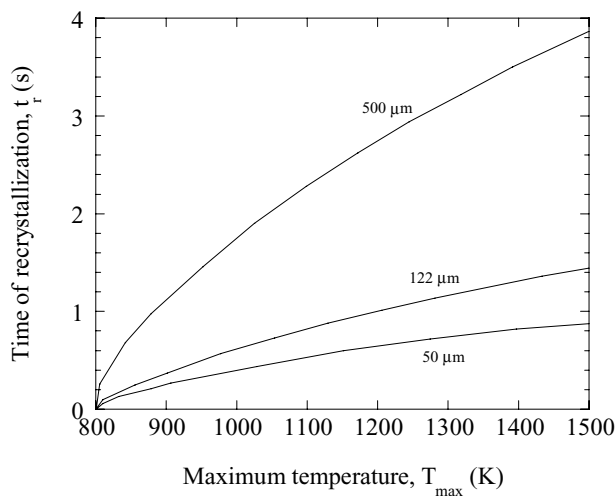


Figure 7 Time of recrystallization as a function of the maximum temperature for as-drawn precursor wires of diameters 500, 122 and 50 μm . See Fig. 6 for experimental conditions.

T_{max} . The grain growth time is longer for 122 μm diameter precursor wire than that of 50 μm diameter for the same T_{max} generated by a laser beam of spot size $2a = 2b = 1$ mm. This indicates that when the same T_{max} is achieved using the same laser beam spot, larger diameter wire exhibits longer hot region. Additionally, the wire of diameter 500 μm was irradiated with a laser beam of much longer length ($2a = 5$ mm) than what was used for the other two wires. This also produces a longer hot region leading to longer grain growth time for 500 μm diameter wire.

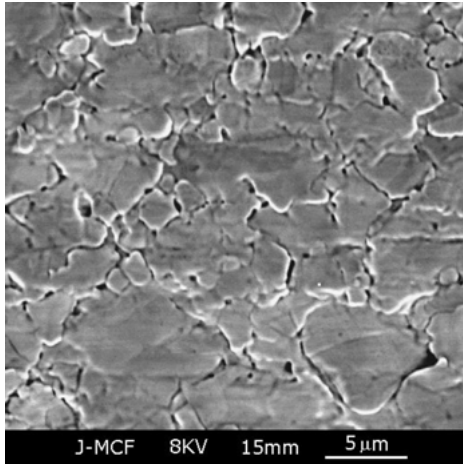
Besides the grain growth time, the initial wire diameter also affects the rate of grain growth. At high temperatures, grooves may form on the surface where grain boundaries intersect the specimen surface, a phenomenon termed thermal grooving [10]. Grain boundary grooves are important in grain growth because they tend to anchor the ends of the grain boundaries. When the average grain size in a metal specimen is very small compared to the dimensions of the specimen, thermal grooving has little effect on the rate of grain growth. However, when the grain size is comparable to the dimensions of the specimen, the grain growth rate decreases [10]. It has been estimated that when the grain size of metal sheets becomes larger than one-tenth of the sheet thickness, the growth rate decreases [11]. The surface area per unit volume increases as the wire diameter decreases, and the effect of thermal grooving becomes more significant as the wire diameter decreases, which increases the resistance for grain growth.

Grain deformation and movement during laser wire drawing process generate specific morphology at the wire surface. The surface images of the as-drawn precursor wires after laser-drawing experiments are shown in Fig. 8 for different values of T_{max} . The grain boundaries are very irregular. No remarkable steps can be observed at the grain boundaries, indicating that little grain boundary sliding occurs during the drawing process. Since the grains in the as-drawn precursor wire recrystallize and grow under tension, the recrystallization and grain growth processes are affected by simultaneous deformation and grain boundary development. The strain rate in the deformation region under the present experimental conditions is mostly in the range of 0.1–0.7 s^{-1} , which is too high for diffusion creep to be the dominant mechanism for deformation. The experimental strain rate and stepless surface morphology suggest that dislocation glide is the dominant deformation mechanism. The constitutive equation describing dislocation creep has the form [12–14]

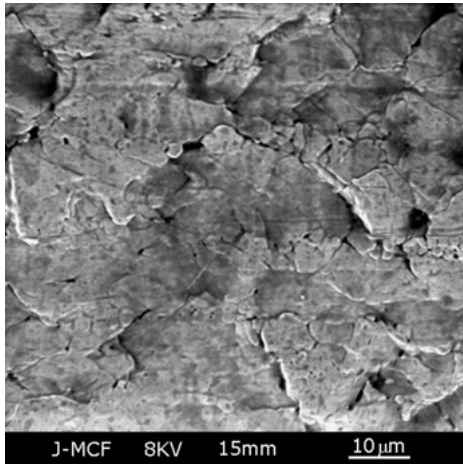
$$\dot{\epsilon} = A \frac{Gb}{kT} \left(\frac{\sigma}{G} \right)^n \exp\left(-\frac{Q}{kT}\right) \quad (7)$$

where $\dot{\epsilon}$ is the strain rate by dislocation creep, Q is the activation energy for creep, A and n are material constants, and all other variables have the same meaning as mentioned earlier. n varies from 3 to 8, with a most commonly used value of 5.

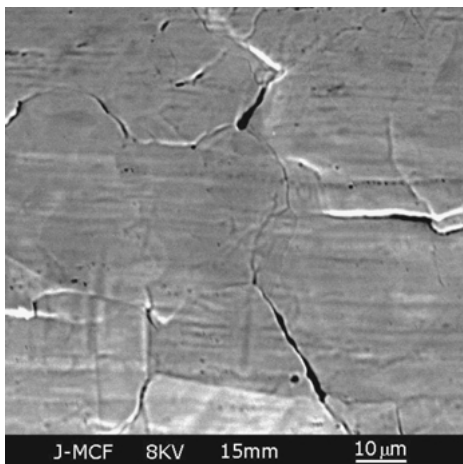
The maximum strain rate in the deformation region, $\dot{\epsilon}_{\text{max}}$, can be calculated using Equation 6 after determining the radius profile for a given laser wire drawing



(a)



(b)



(c)

Figure 8 Surface morphology of as-drawn nickel 200 precursor wires of diameter $500 \mu\text{m}$ after being laser drawn to the same drawing ratio at different laser powers. Grains are irregular. No grain boundary step is observed. Grain size increases with laser power (temperature). $2a = 5 \text{ mm}$, $2b = 0.014 \text{ mm}$, $v_i = 300 \text{ mm/min}$, argon protection. R_a is the cross-sectional area reduction ratio defined as $R_a = (A_i - A_o)/A_i$, where A_i is the cross-sectional area of the initial wire and A_o the area of the output wire after being drawn: (a) Laser-drawn to $411 \mu\text{m}$ ($R_a = 32.4\%$) at $P = 16.6 \text{ W}$ ($T_{\text{max}} = 900 \text{ K}$) showing fine, equiaxed grains, (b) Laser-drawn to $411 \mu\text{m}$ ($R_a = 32.4\%$) at $P = 21.8 \text{ W}$ ($T_{\text{max}} \approx 1091 \text{ K}$) showing larger grains with more nonuniform size than in the case (a), and (c) Laser-drawn to $497 \mu\text{m}$ ($R_a = 1.2\%$) at $P = 26.6 \text{ W}$ ($T_{\text{max}} \approx 1274 \text{ K}$) showing very large grains.

TABLE II Data used to evaluate Equation 8

Shear modulus at room temperature, G_0	76 GPa
Burger's length, b	0.249 nm
Stress factor, n	5
Constant, A	$4 \times 10^{22} \text{ m}^2/\text{s}$
Activation energy, Q	130 kJ/mol

TABLE III Measured tensile stress σ (MPa, relative to the average of the cross-sectional area before and after laser-drawing)

T_{max} (K)	845	900	1115	1091	1274	1366
As-drawn, $d_i = 500 \mu\text{m}$		79.5		63.5	36.3	
As-drawn, $d_i = 122 \mu\text{m}$	91.4		71.6			27.4

condition using the thermomechanical model discussed in [5] Equation 6 shows that $\dot{\epsilon}_{\text{max}}$ is proportional to dr/dx which is approximately proportional to the radius reduction. So $\dot{\epsilon}_{\text{max}}$ increases as the area reduction ratio increases, and reaches its maximum value when the area reduction ratio is maximum. $\dot{\epsilon}_{\text{max}}$ is determined for as-drawn precursor nickel wires of 500 and $122 \mu\text{m}$ diameters at the drawing ratio limits for different values of T_{max} (laser power) and the result is shown in Fig. 8. The drawing limits are also shown. The strain rates are also calculated using Equation 8 based on the drawing stress, temperature and other data given in Tables II and III, and presented in Fig. 9. These strain rates are based on the dislocation creep model, and compare well with the data determined directly from experiments. It was observed that the exact value of the activation energy Q can be varied over a wide range, e.g., 110 – 1500 kJ/mol, to achieve the same trend for the theoretical and experimental strain rates. Q and A are selected as 130 kJ/mol and $4 \times 10^{22} \text{ m}^2/\text{s}$, respectively, in this study to reduce the error between the calculated strain rates and the experimental data points.

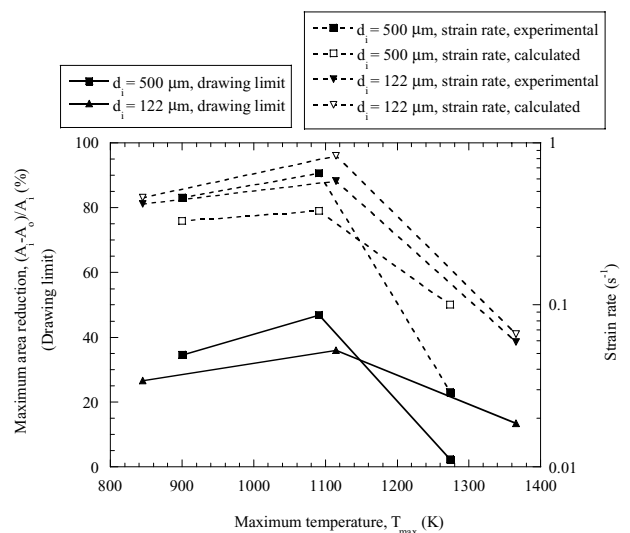


Figure 9 Drawing limit (maximum area reduction ratio at the breakage of the wire) for as-drawn nickel wires at different T_{max} representing under-heating, optimal heating and overheating, and the maximum strain rate at corresponding drawing ratios, determined by both experiment and calculation using Equation 8.

4. Conclusions

Temperature measurement using thermal radiation spectrum verifies a thermomechanical model for laser dieless wire drawing. The temperature profile significantly affects the recrystallization and grain growth of as-drawn precursor nickel 200 wires. The final grain size depends on the maximum temperature, the length of the heated region and on the precursor wire diameter. Grain boundary grooving may be responsible for this size effect on grain growth when the grain size is comparable to the wire diameter. In the neighborhood of the optimal wire temperature and drawing rate, dislocation glide is the dominant deformation mechanism and the maximum strain rate can be described by the constitutive law for dislocation creep. Since the maximum strain rate increases with the drawing ratio, calculated values of the maximum strain rate can be used to correlate the drawing ratio for the laser drawing process.

Acknowledgement

This work was sponsored by the USF Filtration and Separations Group, Inc., Fluid Dynamics Division (now PALL Corporation), Deland, Florida (UCF contract No. 6504887).

References

1. Y. NAMBA, "Laser Forming of Metals and Alloys, LAMP '87: High Temperature Society of Japan, 1987" (High Temperature Society of Japan, c/o Welding Research Institute of Osaka University, 11-1 Mihogaoka, Ibaraki, Osaka 567, Japan) p. 601.
2. D. SCHUÖCKER and K. SCHRÖDER, in Proceedings of LANE'97, Meisenbach, Bamberg, 1997, p. 713.
3. D. SCHUÖCKER, *J. Mater. Process. Technol.* **115** (2001) 104.
4. Y. LI, N. R. QUICK and A. KAR, *ibid.* **123** (2002) 451.
5. *Idem.*, *J. Laser Appl.* **14** (2002) 91.
6. *Idem.*, *Mater. Sci. Eng. B* (submitted).
7. L. MICHALSKI, K. ECKERSDORF and J. MCGHEE, "Temperature Measurement" (John Wiley & Sons, England, 1991) p. 202.
8. F. J. KAHLEN and A. KAR, *High Temp. Mater. Process.* **4** (2000) 161.
9. E. VOCE, *J. Inst. Metals* **74** (1948) 537.
10. R. E. REED-HILL and R. ABBASCHIAN, "Physical Metallurgy Principles" 3rd ed. (PWS-KENT Publishing Company, Boston, 1992) p. 265.
11. P. A. BECK, *Phil. Mag. Supplement* **3** (1954) 245.
12. J. WEERTMAN, *Trans. Metall. Soc. A.I.M.E.* **227** (1963) 1475.
13. A. K. MUCKERJEE, J. E. BIRD and J. E. DORN, *Trans. Amer. Soc. Metals.* **62** (1969) 155.
14. A. ARIELI and A. K. MUKHERJEE, *Metall. Trans. A* **13A** (1982) 717.

Received 14 June

and accepted 17 October 2002